Mass-spectrometric study of the formation, evaporation, and structural properties of doubly charged MgO clusters

Paul J. Ziemann and A. W. Castleman, Jr.
Department of Chemistry, The Pennsylvania State University, University Park, Pennsylvania 16802
(Received 2 April 1991)

Doubly charged $(MgO)_nMg^{2+}$ ($n=4$–172) and $(MgO)_nMg_2^{2+}$ ($n=12$–24) clusters were produced in a gas-aggregation source and studied by using laser-ionization time-of-flight mass spectrometry. The mass spectrum exhibits an interesting dependence on the source conditions, such that it can be changed from one comprised of singly charged clusters to one comprised almost entirely of doubly charged clusters, simply by changing the flow rate of the carrier gas. The abundance of patterns of $(MgO)_nMg^{2+}$ clusters shows that the clusters have cubic structures resembling pieces of the MgO fcc crystal lattice, with the most stable structures being cuboids, and cuboids with an O-atom vacancy or complete terrace. The abundances of $(MgO)_nMg_2^{2+}$ clusters can also be explained in terms of cubic structures, but in this case the O-atom vacancies may be occupied by one or two excess electrons, analogous to a solid-state F center. Simple ionic-model calculations of the structures and relative stabilities of $(MgO)_nMg^{2+}$ clusters are in good agreement with those inferred from the mass spectra. The $(MgO)_nMg^{2+}$ clusters evaporate primarily by losing magnesium and oxygen in equal amounts, similar to the congruent vaporization of solid MgO, yielding clusters of the same series. The mechanism of evaporation is probably a stepwise one in which the movement of atoms or molecules from corners, kinks, and ledges into an adsorbed layer exerts at least partial control over the evaporation rate. At small sizes the doubly charged clusters also appear to undergo Coulomb explosion, in which they fragment to form $(MgO)_n^+$ and $(MgO)_nMg^+$ clusters.

INTRODUCTION

Cluster studies can provide valuable information on the development of the properties of condensed matter from those of isolated atoms or molecules. When studies are performed on species in the gas phase, mass-spectrometric techniques make it possible to identify the clusters present in the sample, and thereby investigate properties as a function of cluster composition and degree of aggregation. By coupling mass spectrometry with various spectroscopic and chemical probes, studies of electronic, structural, and chemical properties have been made on pure and mixed clusters of a large variety of atoms and molecules. Even by itself, mass spectrometry has been a valuable tool in cluster investigations, since the relative intensities of the cluster peaks in a mass spectrum are generally indicative of relative cluster stabilities.[1–3] One very popular system for study has been alkali halide clusters,[4–12] since accurate theoretical calculations have been made by using a simple ionic interaction potential.[3,13,14] The combination of experimental and theoretical investigations has provided insight into the structural, electronic, and fragmentation properties of these clusters.

We have used similar techniques to investigate divalent ionic systems, and have recently reported[15] the results of a study in which we obtained mass spectra of singly charged MgO clusters, and also performed ionic-model and *ab initio* calculations to assist in interpreting the findings. Magnesium oxide is an interesting material for cluster studies, since the known properties of the MgO molecule and the solid state indicate that the bonding in this system undergoes a transition from an approximately equal mixture of ionic and covalent character in the molecule to a predominantly ionic character in the bulk. There is also fundamental and practical interest in many of the properties of the solid, such as its high-temperature stability and vaporization behavior,[16] and catalytic[17] and defect properties.[18] The results of our previous study provide information on the structural properties of MgO clusters, the development of ionic bonding character, and fragmentation. We have continued to pursue these and other important questions about MgO and related compounds, and here we report on a study of doubly charged MgO clusters. The mass spectra extend to significantly larger cluster sizes (comparable to the sizes that have been obtained for the alkali halides) than they did for the singly charged MgO clusters, and also exhibit much richer patterns. The mass spectra contain more detailed information on structural properties than we could obtain from our earlier investigation and, when compared to the mass spectra of the singly charged clusters, they allow us to ascertain the effect of charge state on cluster structure. The presence of an extra charge also opens additional fragmentation channels for the doubly charged clusters, such that dissociation to singly charged fragments can occur when the cohesive forces in a cluster are overcome by the repulsive Coulomb interaction between the two positive charges. This so-called "Coulomb explosion" has been the object of much study,[19–21] and its occurrence in doubly charged MgO clusters is apparent from the mass spectra. Our results also suggest a

mechanism for the evaporation of MgO clusters and provide another opportunity to investigate the utility of simple ionic-model calculations.

EXPERIMENT

The experimental apparatus has been described in detail elsewhere.[22] Basically, inside a liquid-nitrogen-cooled source chamber where the pressure is about 5 Torr, magnesium metal at 750–850 °C is evaporated from a boron nitride crucible that is resistively heated by a tungsten wire and heat shielded around the circumference and on the bottom by tantalum sheet. The metal vapor is entrained in 1000–4000 sccm (standard cubic centimeter per minute) of cold He and up to 5 sccm of N_2O, whereupon it cools and undergoes concomitant clustering reactions. Gas exits the source chamber and travels through an inverted U-tube into a flow tube at about 0.5 Torr pressure, where an additional He flow is introduced to maintain the total flow close to 4000 sccm. Most of the gas is pumped away by a roots pump located at the end of the flow tube, but a small fraction passes through an on-axis hole in a sampling cone and into the ionization region. The sampled flow tube effluent is then ionized by a focused beam of either 308 nm (XeCl excimer gas, 4.03 eV photons) or 248 nm (KrF excimer gas, 5.00 eV photons) wavelength radiation from an excimer laser operating at 10 Hz, and the ions are accelerated to about 2-kV energy before entering the detection region for time-of-flight mass analysis. Typical laser powers, averaged over a 1-cm^2 iris through which the beam passes prior to entering the vacuum chamber, are about 10–40 mJ/pulse. Average power densities of 0.3–1.2 MW/cm^2 result from the ~30 nsec pulses. However, because the beam is focused (~2-mm beam waist), the power densities in the ionization region are much higher. Fourier transform techniques were used to remove high-frequency noise from the mass spectra, and a gently sloping baseline was subtracted by polynomial curve fitting. Great care was taken to ensure that these procedures had no significant effect on the relative cluster peak heights.

IONIC-MODEL CALCULATIONS

The potential energies of $(MgO)_nMg^+$ clusters were calculated by using an ionic model, in which a cluster is assumed to be composed of rigid ions (here Mg^{z+} and O^{z-}) that interact by a pairwise Born-Mayer potential of the form

$$V_{ij}=Z_iZ_je^2/4\pi\epsilon_0R_{ij}+\lambda\exp(-R_{ij}/\rho)\ , \qquad (1)$$

where Z_i and Z_j are the changes (in units of e) on two interacting ions, e is the elementary charge, ϵ_0 is the permittivity of vacuum, R_{ij} is the distance between the ions, and ρ and λ are two parameters that can be obtained from properties of the monomer and/or solid state. The cluster potential energy relative to the ions at infinite separation is found by summing V_{ij} over all ions ($i\neq j$).

Calculations were made with charges of ±1 on the constituent ions and the parameters: $\rho=0.301$ Å and $\lambda=1226$ eV, which were obtained by fitting to the properties of the solid. The value of ρ was taken from the Gilbert-type exponential repulsive term in a more complex pair potential used to study a number of properties of solid MgO.[23] This value has also been recommended for MgO lattice-energy calculations with a Born-Mayer potential.[24] The corresponding value of λ was calculated by using ρ, ionic charges of ±2,[25,26] the crystalline MgO bond distance of 2.10 Å,[27] and equations relating these quantities.[28] Although the bulk solid apparently has ionic charges close to ±2, our previous calculations made on $(MgO)_n$ and $(MgO)_nMg^+$ clusters suggest that these values are too large for calculating cluster structures and stabilities, and that charges closer to the ±0.74 values of the MgO monomer (calculated from the dipole moment and bond length) are more appropriate. In that study, cubic structures were obtained when the ionic constituents were assigned charges of ±1, which is in agreement with the structures indicated by the mass spectral abundance patterns of singly charged MgO clusters, whereas noncubic structures were obtained when the charges were ±2. We therefore used single charges in the present calculations.

The minimum potential energy for a particular cluster was found by specifying an initial configuration and then moving the ions, one at a time, under the constraint that the potential energy be lower after each step. A step length of 0.01 Å gave adequate sensitivity, while keeping calculation times to a minimum. The calculation was stopped when the decrease in potential energy over ten iterations was less than 0.005 eV, where one iteration is defined as the stepping of all the ions along all three Cartesian coordinates.

In our earlier investigation of $(MgO)_n$ and $(MgO)_nMg^+$ clusters, we started the calculations from a variety of initial configurations that were chosen on the basis of the most stable structures observed in NaCl cluster calculations made with a Born-Mayer potential.[3] When we used single charges and the same set of parameters listed above, we generally found that cubic geometries were preferred, especially once n was larger than about 10. For this reason, we used only cubic structures for initial configurations in the calculations described here (typically 5 or 6 of the most compact structures for each cluster size), in which we extended our previous results on $(MgO)_nMg^+$ clusters from $n\leq32$ to $n\leq50$.

For each cluster size, we obtained potential energy minima corresponding to a number of different geometries. These were used to calculate dissociation energies by assuming that all clusters of a given size have the structure and potential energy of the lowest potential energy configuration, and that $(MgO)_nMg^+$ clusters dissociate by the loss of a MgO monomer. The dissociation energy is then the difference between the potential energies of the parent and products, and is a measure of the relative cluster stability towards fragmentation by the chosen pathway.

RESULTS

Mass spectra

When we operate our gas-aggregation source with pure He carrier gas we do not observe Mg clusters larger than

the dimer, but upon adding a few sccm of N_2O we generate moderately high intensities of MgO clusters. Singly charged $(MgO)_n^+$ and $(MgO)_nMg^+$ clusters are observed when the He flow through the source is greater than about 2500 sccm, but as the flow is decreased by about 500–1000 sccm, doubly charged $(MgO)_nMg^{2+}$ clusters appear and eventually dominate the mass spectrum. The He flows over which the transition occurs depend on the source temperature, but are usually in the 1500–2500 sccm range. Within either the high flow (only singly charged clusters present) or low flow (primarily doubly charged clusters present) regimes, the cluster distribution shifts to larger sizes as the flow of He or N_2O through the source is increased, and so by adjusting these two variables we are able to maximize cluster intensities in different size ranges.

One might expect that the ionization conditions would have an important effect on the cluster distribution, such that it might be possible to shift from singly to doubly charged clusters by increasing the laser power. However, as reported elsewhere,[15] when working in the high flow regime we find that increasing the laser power only increases the intensities of $(MgO)_n^+$ clusters relative to $(MgO)_nMg^+$ clusters and shifts the distribution to smaller sizes. Over the range of laser powers investigated, the change in the distribution from singly to doubly charged clusters depends primarily on the He flow, and not upon the ionization conditions.

In Figs. 1 and 2 we show mass spectra obtained in the low flow regime for ionization at 308 and 248 nm, respectively, with the source conditions adjusted to maximize the distributions in different size ranges. The primary cluster series observed at either wavelength are doubly charged $(MgO)_nMg^{2+}$ clusters, with n up to about 60 at 308 nm and 170 at 248 nm. Doubly charged $(MgO)_nMg_2^{2+}$ clusters are observed at 308 nm, and singly charged $(MgO)_nMg^+$ and $(MgO)_n^+$ clusters with n up to about 10–20 appear as minor series in the mass spectra at both wavelengths. At 248 nm there are also small peaks corresponding to $(MgO)Mg_2^+$ and $(MgO)_2Mg_2^+$, and an apparent contribution from $(MgO)_{12}Mg_2^{2+}$ that leads to a local maximum at $(MgO)_6Mg^+$, instead of at the usual $(MgO)_5Mg^+$.

In Figs. 3(a) and 3(b) we show mass spectra obtained at 308 nm, which have been expanded to show the less abundant clusters more clearly. The spectra were obtained under the same source conditions, but the one in Fig. 3(b) was obtained at twice the laser power as that in Fig. 3(a). All of the peaks are easy to assign, except for one with a mass of about 72 that appears between $(MgO)Mg^+$ and $(MgO)_2^+$. This peak could correspond to $(MgO)_3Mg^{2+}$, but it appears only rarely at 308 nm and not at all 248 nm, despite the fact that $(MgO)_4Mg^{2+}$ is relatively intense at the latter wavelength. Furthermore, it is more intense than some larger $(MgO)_nMg^{2+}$ cluster peaks, and yet almost disappears at higher laser power, whereas they do not. It is most likely either Mg_3^+ or a contaminant. This peak is primarily of interest in determining the lower size limit of the $(MgO)_nMg^{2+}$ cluster distribution and, for the reasons just mentioned, we think that the smallest $(MgO)_nMg^{2+}$ cluster is probably $(MgO)_4Mg^{2+}$. A more important complication in this mass spectrum is that, for even values of n, $(MgO)_nMg_2^{2+}$ and $(MgO)_{n/2}Mg^+$ clusters have the same mass-to-charge ratio, and therefore appear at the same place in the mass spectrum. This makes the assignment of some of the abundance maxima and the smallest cluster size uncertain for $(MgO)_nMg_2^{2+}$ clusters. If the solid peaks in Figs. 1 and 3(a) contain no contributions from $(MgO)_nMg^+$ clusters, then the peaks correspond to $(MgO)_nMg_2^{2+}$ clusters with $n=2$, 4, 6, 8, 10, 12, 13, 14, 15, etc., and therefore no odd numbered clusters are

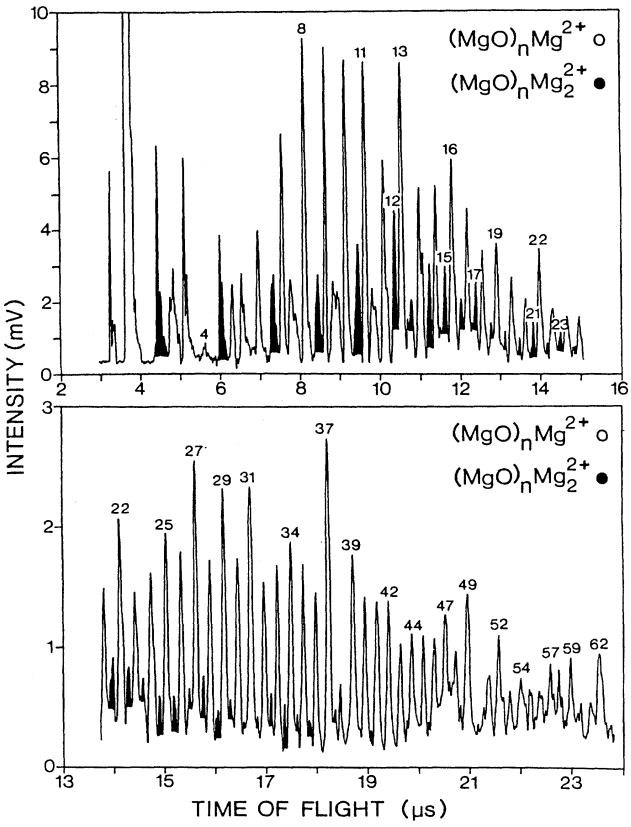

FIG. 1. Time-of-flight mass spectra of MgO clusters obtained by using 308-nm wavelength radiation for ionization (XeCl excimer gas, 4.03-eV photons, 20 mJ/pulse) and source conditions optimized for different size regimes. The primary series of open peaks corresponds to $(MgO)_nMg^{2+}$ clusters, for which the abundance maxima and smallest cluster, $(MgO)_4Mg^{2+}$, are numbered. The solid peaks to the left of $(MgO)_{11}Mg^{2+}$ correspond to $(MgO)_nMg^+$ clusters with $n=1$–5, and those to the right are due to $(MgO)_nMg_2^{2+}$ and $(MgO)_{n/2}Mg^+$ (for even values of n) clusters. The solid peaks that we identify as true abundance maxima for $(MgO)_nMg_2^{2+}$ clusters are numbered (see text for details). The small open peaks to the right of odd numbered $(MgO)_nMg^{2+}$ clusters correspond to $(MgO)_{(n+1)/2}^+$ clusters, and the large off-scale peak is due to Mg_2^+. The less abundant clusters can be seen in an expanded view in the spectra shown in Fig. 3.

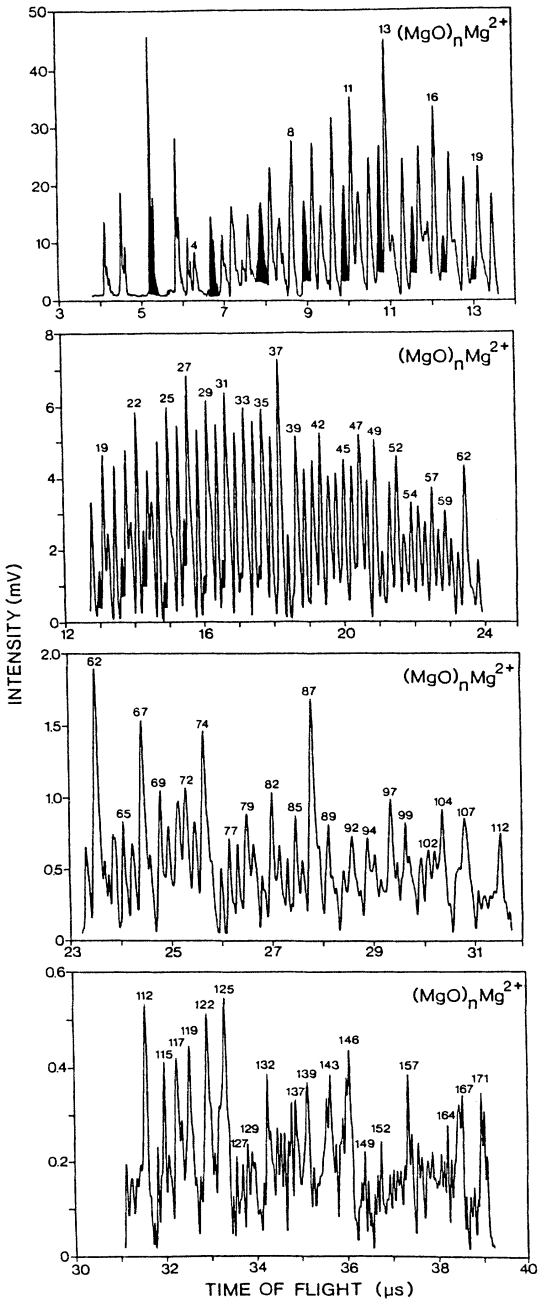

FIG. 2. Time-of-flight mass spectra of MgO clusters obtained by using 248-nm wavelength radiation for ionization (KrF excimer gas, 5.00-eV photons, 10 mJ/pulse) and source conditions optimized for different size regimes. The primary series of open peaks corresponds to $(MgO)_nMg^{2+}$ clusters, for which the abundance maxima and smallest cluster, $(MgO)_4Mg^{2+}$, are numbered. The solid peaks to the right of even numbered $(MgO)_nMg^{2+}$ clusters correspond to $(MgO)_{n/2}Mg^{+}$ clusters, with an apparent contribution to $(MgO)_6Mg^{+}$ from $(MgO)_{12}Mg_2^{2+}$ (see text for details). The small open peaks to the right of odd numbered $(MgO)_nMg^{2+}$ clusters are due to $(MgO)_{(n+1)/2}^{+}$ clusters, and the five peaks to the left of $(MgO)_4Mg^{2+}$ correspond MgO^+, Mg_2^+, $(MgO)Mg^+$, $(MgO)_2^+$, and $(MgO)Mg_2^+$. The abundance patterns for the singly charged clusters at 248 nm are similar to those obtained at 308 nm, which are shown in an expanded view in Fig. 3.

present for $n < 12$. But because there is no reason to expect such an extreme odd-even alternation in the stabilities of these clusters, it is more likely that there are no $(MgO)_nMg_2^{2+}$ clusters present for $n < 12$, and that the peaks at 2, 4, 6, 8, and 10 correspond instead to $(MgO)_{n/2}Mg^+$ clusters. The $(MgO)_{12}Mg_2^{2+}$ peak apparently has only a small contribution from $(MgO)_6Mg^+$ clusters, since its intensity decreases significantly at higher laser power (Fig. 3), whereas the $(MgO)_nMg^+$ cluster peaks to the left of it change very little [except for $(MgO)Mg^+$]. The smallest $(MgO)_nMg_2^{2+}$ cluster therefore appears to be $(MgO)_{12}Mg_2^{2+}$.

The $(MgO)_nMg^{2+}$ mass spectra contain many abun-

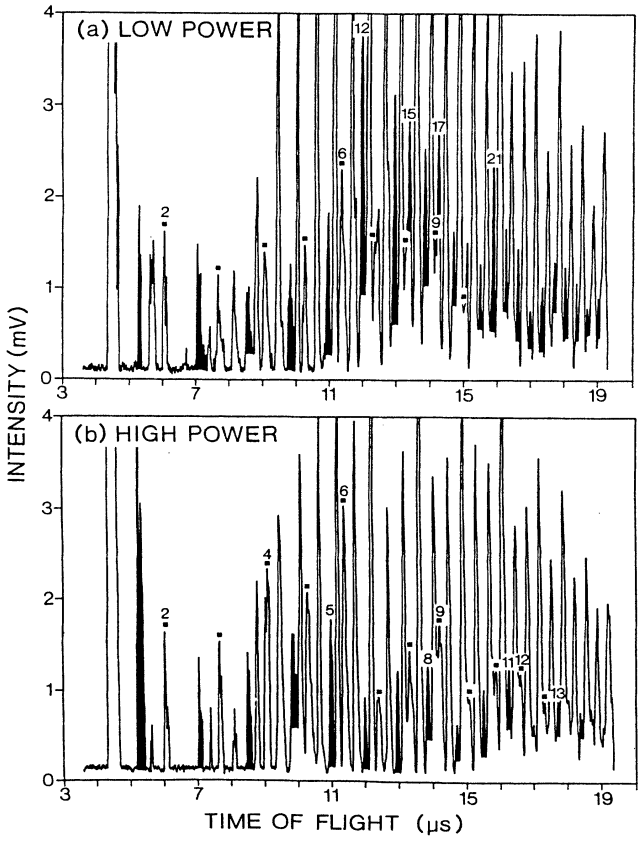

FIG. 3. Time-of-flight mass spectra of MgO clusters obtained by using (a) 20 mJ/pulse and (b) 40 mJ/pulse of 308-nm wavelength radiation for ionization (XeCl excimer gas, 4.03-eV photons). In both spectra the primary series of open peaks corresponds to $(MgO)_nMg^{2+}$ clusters, and the open peaks with a dot above them are due to $(MgO)_n^+$ clusters. In spectrum (a) the solid peaks to the left of $(MgO)_6^+$ correspond to $(MgO)_nMg^+$ clusters with $n = 1$–5, and those to the right are due to $(MgO)_nMg_2^{2+}$ and $(MgO)_{n/2}Mg^+$ (for even values of n) clusters. The solid peaks that we identify as true abundance maxima for $(MgO)_nMg_2^{2+}$ clusters are numbered (see text for details). In spectrum (b) the solid peaks correspond entirely to $(MgO)_nMg^+$ clusters. In both spectra the large off-scale peak is due to Mg_2^+, and the peak between $(MgO)Mg^+$ and $(MgO)_2^+$ is probably a contaminant.

dance maxima, which are essentially independent of the wavelength used for ionization. The only differences are that maxima occur at 34 and 44 at 308 nm, but at 33, 35, and 45 at 248 nm. In the mass spectra obtained at 248 nm the peak shapes of $(MgO)_nMg^{2+}$ clusters with odd n are sometimes affected by overlap with smaller $(MgO)_{(n+1)/2}^{+}$ peaks that follow them by 8 amu/charge [two adjacent $(MgO)_nMg^{2+}$ peaks are separated by 20 amu/charge]. The peaks are well resolved when n is less than about 25, but for larger clusters a hump appears on the right side of the $(MgO)_nMg^{2+}$ peaks, leading to wider peaks for odd than even values of n. The overlap may also increase the apparent intensities of $(MgO)_nMg^{2+}$ clusters with odd n values, possibly leading to some of the observed abundance maxima. However, any effect is probably negligible for n greater than about 40–50, since by this size $(MgO)_nMg^{2+}$ peaks of similar height have similar widths regardless of whether n is odd or even. The maxima observed for $(MgO)_nMg^{2+}$ clusters obtained at 308 nm are not affected by peak overlap, since the intensities of $(MgO)_n^{+}$ clusters are much smaller than at 248 nm. The resolution at 308 nm is high enough to see that the intensities of $(MgO)_n^{+}$ clusters are negligible once n is greater than about 10–15 and, in addition, the $(MgO)_nMg^{2+}$ peaks have no humps and similar widths for odd and even n. Since the maxima observed at 248 and 308 nm are almost identical, it appears that the only effect of peak overlap on those at 248 nm might be the shift from 34 and 44 to 33, 35, and 45. In Table I all of the maxima observed for $n \leq 50$ are listed to enable ready comparison with the results of the ionic-model calculations. Also listed are some of the most intense abundance maxima observed for larger clusters, and proposed cluster structures based on the face-centered cubic geometry of crystalline MgO.

Ionic-model calculations

The results of our rigid ion-model calculations on $(Mg^{+}O^{-})_nMg^{+}$ clusters indicate a preference for cubic structures, and some slightly distorted forms of these, similar to the results of $(NaCl)_nNa^{+}$ cluster calculations.[3,13] The most stable $(Mg^{+}O^{-})_nMg^{+}$ structures are usually calculated to be cubic, but occasionally structures containing stacks of hexagonal or octagonal rings have slightly lower potential energies. The latter structures can be pictured as stacks of 3×2 or 4×2 rectangles, respectively, which open up to form stacks of rings. Once the clusters contain about 20 atoms, the cubic structures are always the most stable ones. The $(Mg^{+}O^{-})_nMg^{+}$ cluster dissociation energies, calculated for the loss of MgO monomer, are shown in Fig. 4. There is good agreement between the maxima in dissociation energies, which are a measure of cluster stability, and the abundance maxima in the $(MgO)_nMg^{2+}$ mass spectra.

TABLE I. Mass spectral abundance maxima and proposed structures of $(MgO)_nMg^{2+}$ clusters. The list includes all the maxima observed for $n \leq 50$, for comparison with the results of the ionic-model calculations, and the most intense maxima observed for $n > 50$.

$(MgO)_nMg^{2+}$	Structure[a]	$(MgO)_nMg^{2+}$	Structure
8	3×3×2−1	57	5×5×4+5×3
11	4×3×2−1	59	6×5×4−1
13	3×3×3	62	5×5×5
16	3×3×3+3×2	67	9×5×3
19	4×3×3+3×1	74	6×5×5−1
22	5×3×3	82	11×5×3
25	5×3×3+3×2	87	7×5×5
27	5×3×3×3+5×2	97	13×5×3
29	5×4×3−1	104	7×6×5−1
31	7×3×3	107	6×6×6−1
	4×4×4−1	112	9×5×5
34[b]	5×4×3+3×3	122	7×7×5
37	5×5×3	125	7×6×6−1
39	5×4×4−1	132	8×6×5+5×5
42	5×5×3+5×2	139	8×7×5−1
44[b]	6×5×3−1	143	8×6×6−1
47	6×4×4−1	146	7×7×6−1
	5×5×3+5×4	157	9×7×5
49	5×5×4−1	167	8×7×6−1
52	7×5×3	171	7×7×7

[a]The $a \times b \times c$ designation corresponds to a cuboid structure with a, b, and c atoms along each edge, the −1 refers to an O-atom vacancy, and the $a \times d$ designation refers to a complete terrace on an $a \times b$ or $a \times c$ face of a cuboid. When more than one structure can be used to explain the occurrence of a maximum, the most symmetric and/or compact one is listed.

[b]The list includes the maxima that appear at 34 and 44 in the spectrum obtained at 308 nm, rather than those that appear at 33, 35, and 45 in the spectrum obtained at 248 nm, since the latter may be affected by overlap with $(MgO)_{(n+1)/2}^{+}$ peaks (see text for details).

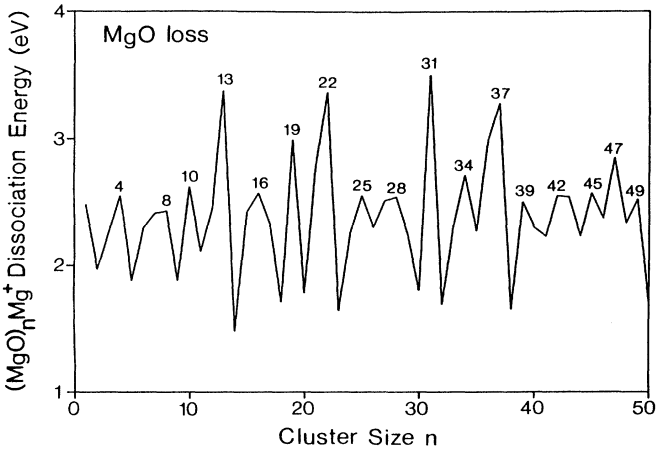

FIG. 4. Dissociation energies of $(Mg^+O^-)_nMg^+$ clusters obtained from the results of ionic-model calculations, assuming dissociation by the loss of a MgO molecule.

DISCUSSION

Formation of doubly charged MgO clusters

In a typical cluster mass spectrum one expects to see primarily singly charged clusters, such as the $(MgO)_n^+$ and $(MgO)_nMg^+$ series that we observe under high flow conditions. Sometimes multiply charged clusters are also present, but they usually appear only at large sizes (the higher the charge, the larger the minimum cluster size, due to increased Coulomb repulsion) and in significantly lower abundances. It therefore came as a complete surprise when we observed that our mass spectrum could be shifted from one comprised only of singly charged clusters to one comprised almost entirely of doubly charged clusters, simply by changing the flow of carrier gas. Since the shift can be affected by varying the source conditions, while maintaining constant laser power, it must be due to differences in the compositions of clusters generated at high and low He flows. The clusters exiting the source under low flow conditions probably contain more excess metal than at high flow, and this decreases their ionization potentials enough to allow multiple ionization [the photoionization threshold of MgO(s) is about 10 eV,[29] whereas the ionization potential of a Mg atom and the work function of Mg(s) are about 7.65 and 3.7 eV,[27] respectively].

Because the clusters have cubic structures, usually only one or two of the excess Mg atoms can occupy sites in the lattice where they will have a high binding energy (i.e., high coordination). The remainder must bind to one or two O atoms, and perhaps to other Mg atoms through relatively weak metal-metal interactions. These atoms would be expected to readily evaporate after ionization, carrying away excess energy, and also excess charge if the cluster has been more than doubly ionized. Once the clusters reach the $(MgO)_nMg^{2+}$ composition they lose Mg and O in equal amounts, probably as MgO or $2Mg+O_2$, while maintaining the same charge state.

The proposed role for excess Mg in this mechanism is supported by the observation that $(MgO)_nMg_2^{2+}$ clusters are present at low flow, whereas at high flow we never detect clusters containing more than one excess metal atom. In addition, the lower stabilities attributed to $(MgO)_nMg_2^{2+}$ clusters, compared to $(MgO)_nMg^{2+}$ clusters, are apparent from their lower abundances and the fact that they disappear when fragmentation is induced by doubling the laser power (Fig. 3), while the $(MgO)_nMg^{2+}$ distribution is only slightly affected.

We also considered the possibility that $(MgO)_nMg^{2+}$ and $(MgO)_nMg_2^{2+}$ clusters might be generated [from $(MgO)_n^+$ and $(MgO)_nMg^+$ clusters, respectively] by the loss of an electron and an O atom. This would be analogous to the mechanism by which singly charged, metal-rich alkali halide clusters are formed from the stoichiometric neutrals.[5] However, when we tried to create doubly charged clusters from the $(MgO)_n^+$ and $(MgO)_nMg^+$ clusters produced at high flow by increasing the laser power, the singly charged clusters merely fragmented to smaller sizes. This result leaves little doubt that the doubly charged MgO clusters are formed from more metal-rich species.

It is tempting to think that the $(MgO)_nMg^{2+}$ clusters formed in these experiments are composed of closed-shell Mg^{2+} and O^{2-} ions, and can therefore be described by the formula $(Mg^{2+}O^{2-})_nMg^{2+}$. But since the results of our previous calculations[15] suggest that the magnitude of the charges on the ions is significantly less than 2, at least for clusters containing up to about 64 atoms (the largest size examined), we believe that this is too simplistic a picture. It is probably best to consider this formula as an approximate description of the charge states of the constituent atoms: one which is inadequate for small clusters, but becomes more accurate with increasing cluster size. It is still an open question as to how large these clusters must be to attain bulklike electronic properties.

We are uncertain as to why substantially different neutral cluster compositions are obtained in the high and low He flow regimes, but the most likely explanation is that the flow affects the clustering process through its influence on the pressure or residence time of clusters in the source. Cluster growth is generally enhanced at higher pressures, as increased collisional cooling lowers cluster temperatures, thereby reducing evaporation. We would therefore expect to produce metal-rich clusters at high flow, where the higher pressure (about twice that at low flow) can stabilize the weakly bound excess Mg atoms. Instead we produce them primarily at low flow, although we do observe the effect of pressure on growth in both regimes, as evidenced by the fact that the singly and doubly charged cluster distributions can each be shifted to larger sizes by increasing the He flow. It is more likely that the differences in cluster compositions are due to differences in the residence times, which depend on the ratio of the pressure and mass flow rate, and the degree of mixing. If the clusters are well mixed under all flow conditions, then calculated residence times are almost constant over the entire range of flows since the pressure is approximately proportional to the mass flow

rate. We believe, rather, that mixing is not always complete, and that abrupt changes occur in flow patterns inside the source. Within either flow regime, metal-rich clusters are probably formed in the immediate vicinity of the crucible, where the $[Mg]/[N_2O]$ ratio is large. At high flow, these clusters are probably mixed throughout the rest of the source, where they obtain stoichiometric or nearly stoichiometric compositions through reactions with vapor that has a much lower $[Mg]/[N_2O]$ ratio. At low flow, strong vertical convection currents generated by the crucible heater apparently drive metal-rich clusters out of the source before they have time to become more fully oxidized. If we assume that clusters produced under low flow conditions travel to the source exit hole within a cylindrical volume that has the same diameter as the crucible (or the exit hole, since they are about equal), whereas clusters produced at high flow traverse the entire volume of the source, then based on the ratio of the volumes occupied by the clusters while in the source, the clusters formed at high flow will have residence times that are about one hundred times longer than those of clusters formed at low flow.

In addition to being dominated by doubly charged clusters, the mass spectra also exhibit rich patterns of cluster abundances. The most striking features in the spectra are the abundance maxima, or so-called "magic numbers," which appear because clusters that are more stable than their neighbors are more resistant to fragmentation and thus acquire enhanced relative abundances. The role of fragmentation has been clearly demonstrated for alkali halide clusters produced by sputtering,[6] since mass spectra obtained a few tenths of a μs after production show a smooth cluster distribution, whereas magic numbers appear when the clusters are allowed to fragment for a few hundred μs before a spectrum is collected. In our experiments fragmentation can occur in both the source and ionization region. In the source, the formation of strong metal-oxygen bonds during cluster growth releases large amounts of heat into the clusters that could lead to fragmentation, but a simple calculation similar to that made on transition-metal oxide clusters generated by laser vaporization[30] suggests that the clusters are cooled by collisions with carrier gas before a significant amount of evaporation can occur. The clusters can be reheated in the ionization region by the absorption of photons, in which case they can only cool by evaporation since the pressures are too low for collisional cooling. Evaporation can occur before and after ionization, but model calculations of the fragmentation of multiphoton ionized FeO clusters indicate that most evaporation takes place after ionization.[30] This is primarily because the neutrals must fragment and then ionize within the approximately 30-ns laser pulse, whereas the ions have about 1 μs to fragment in the acceleration region. That most fragmentation follows ionization in our experiments is also indicated by the presence of excess metal in the neutral clusters, which allows them to become doubly ionized, and then subsequently evaporates. Fragmentation of $(MgO)_nMg^{2+}$ clusters probably occurs after the excess metal is gone, leading to enhanced relative abundances for exceptionally stable clusters.

Mass spectra and ionic-model calculations

The abundance patterns that we observe for $(MgO)_nMg^{2+}$ clusters can be explained in terms of the relative stabilities of simple cubic structures, which resemble pieces of the fcc MgO crystal. The magic numbers correspond to clusters with compact cuboid structures, and also cuboids with a single O-atom vacancy or a complete terrace. These three types of structures can be written as (1) $a\times b\times c$, (2) $a\times b\times c-1$, and (3) $a\times b\times c+a\times d$, whereas the $a\times b\times c$ designation refers to a cuboid with a, b, and c atoms along each edge, the -1 refers to an O-atom vacancy, and the $a\times d$ designation refers to a complete terrace on an $a\times b$ or $a\times c$ face of a cuboid. Because of their stoichiometries, all of the clusters contain an odd number of atoms. Therefore, a, b, and c must all be odd for structure (1), $a\times b\times c$ must be even for structure (2), and if $a\times b\times c$ is even for structure (3), then $a\times d$ must be odd, and vice versa. The most intense abundance maxima (Table I) correspond to clusters with one of the first two types of structures, and the less intense maxima are due primarily to clusters of the third type. In this latter class of structures, terraces containing three atoms along one dimension are prominent for $n\leq 34$, those with five atoms for $n\geq 27$, and those with seven atoms for $n\geq 115$. For many of the maxima there is often more than one structure that can be used to explain the exceptional stability of the corresponding cluster, but the predominant isomers are probably the most symmetric and compact ones. As indicated by the results of our ionic-model calculations, clusters with these two properties tend to have the highest binding energies. Not only can all of the observed maxima be explained in terms of the three types of structures described above, but there are few instances where a structure that falls into one of these classes does not appear as a maximum.

The magic numbers observed in the $(MgO)_nMg^{2+}$ mass spectra are the same as those we reported earlier for singly charged $(MgO)_nMg^{+}$ clusters ($n\leq 31$, with lone peaks at 37 and 62) ionized at 308 nm, except that in the latter case none appears at 27. The same ones have been observed for $(MgO)_nMg^{+}$ clusters generated by sputtering,[31] with cluster sizes up to about 30–40. Because much less data are available for $(MgO)_nMg^{+}$ than for $(MgO)_nMg^{2+}$ clusters, we cannot make a very extensive comparison between the two series. However, it appears that at least for $8\leq n\leq 31$ the addition of an extra charge has little effect on the cluster structures, since within this size regime the maxima are nearly the same for either charge state. At sizes smaller than about 8 the extra charge evidently destabilizes the doubly charged clusters, since none are observed for $n<4$, and the maximum normally present at 5 for the singly charged clusters is absent. These results are indicative of the strong bonding in MgO clusters (single-bond energies probably lie between the 2.6-eV monomer[32] and the 1.7-eV solid-state[27] values), which is not significantly affected by Coulomb repulsion until the clusters reach very small sizes. By comparison, sodium clusters have binding energies of about 0.8 eV, and Na_n^{2+} clusters are only observed in

mass spectra for $n \geq 27$.[21]

Comparisons can also be made between the mass spectra of $(MgO)_nMg^{2+}$ clusters and those that we reported earlier for singly charged $(MgO)_n^+$ clusters ($n \leq 90$), in which the magic numbers correspond almost entirely to cuboid structures, where the product of $a \times b \times c$ must be an even number. The vacancy structures ascribed to $(MgO)_nMg^{2+}$ clusters can be generated from these by removing an O atom. In many cases, if a maximum occurs at a particular value of n in the $(MgO)_n^+$ mass spectrum, then there is one at $n-1$ in the $(MgO)_nMg^{2+}$ mass spectrum.

Mass spectra of doubly charged $(CaO)_nCa^{2+}$ clusters ($n \leq 70$) have been reported recently,[33] and the abundance minima explained in terms of the instabilities of the corresponding clusters relative to those with cuboid structures. However, there is no discussion of the maxima observed, and it is difficult to determine their locations from the mass spectrum presented. We have produced $(CaO)_nCa^{2+}$ clusters up to about 100, and the maxima are similar to those of $(MgO)_nMg^{2+}$ clusters.[34]

The abundance maxima of $(MgO)_nMg^{2+}$ clusters are also similar to those observed in the mass spectra of singly charged alkali halide clusters with the stoichiometries $(MX)_nM^+$ and $(MX)_nX^-$ (M denotes alkali metal, X denotes halide), produced by laser vaporization.[12] In spite of the fact that the bulk crystal structures of some of the alkali halides investigated are bcc, rather than fcc, their cluster mass spectra only differ from each other in a few minor respects that can be attributed to differences in lattice energies and ionic radii. The most pronounced mass spectral features are found in the alkali halides with the highest lattice energies and, for a given alkali halide, the $(MX)_nM^+$ and $(MX)_nX^-$ spectra are most similar when the cation and anion radii are about the same, so that the ions can exchange places in the cluster without significantly affecting the structure. In this respect, a useful quantity for structural comparisons is the ratio of the ionic radii of the major and minor cluster components, calculated by using bulk values. For example, for $(NaCl)_nNa^+$ and $(NaCl)_nCl^-$ clusters the pertinent radius ratios[27] are r_{Na^+}/r_{Cl^-} (0.54) and r_{Cl^-}/r_{Na^+}, respectively. The lattice energy (and atomization energy) of MgO is much larger than that of any of the alkali halides, but the radius ratio (0.50 for $r_{Mg^{2+}}/r_{O^{2-}}$, 0.47 for r_{Mg^+}/r_{O^-}) is close to that of NaCl, for which cluster mass spectra have been obtained up to about the same size as for $(MgO)_nMg^{2+}$ clusters. Most of the magic numbers in the $(MgO)_nMg^{2+}$ mass spectra are present in both the $(NaCl)_nNa^+$ and $(NaCl)_nCl^-$ spectra, but the correspondence is slightly better with $(NaCl)_nCl^-$ clusters, which exhibit a greater preference for vacancy structures than $(NaCl)_nNa^+$ clusters. This is interesting, since ionic radii considerations suggest that $(MgO)_nMg^{2+}$ and $(NaCl)_nNa^+$ clusters should have more similar structural preferences.

In spite of the fact that our ionic-model calculations on MgO clusters showed that covalent interactions must be included in order to obtain quantitatively accurate results, we also found that the relative cluster stabilities calculated by using charges of ± 1 on the constituent ions [i.e., $(Mg^+O^-)_n$ and $(Mg^+O^-)_nMg^+$ clusters] were in good qualitative agreement with the mass spectral abundances of the singly charged MgO clusters. Since we now have produced much larger metal-rich clusters, and the magic numbers of the clusters are not affected by the charge state, we have extended our calculations in order to compare the calculated stabilities of $(Mg^+O^-)_nMg^+$ clusters with the $(MgO)_nMg^{2+}$ cluster abundances. Although the fragmentation of $(MgO)_nMg^{2+}$ clusters probably does not occur in a single step, and the actual species desorbed may be Mg atoms and O_2 molecules instead of MgO molecules (these points are discussed later), the dissociation energies calculated for the loss of MgO molecules should still be useful quantities for comparisons of relative cluster stabilities. The similarities in the magic numbers observed for alkali halide and $(MgO)_nMg^{2+}$ clusters, in spite of the fact that the alkali halides lose monomers and dimers,[11] support this assumption.

The $(Mg^+O^-)_nMg^+$ structures calculated to be the most stable are the same three types described above, and the agreement between the calculated stability maxima (Fig. 4) and the maxima in the cluster mass spectra is quite good. One discrepancy is that, whereas a maximum occurs at 28 in the calculations, maxima occur at 27 and 29 in the mass spectra. Since a maximum is usually observed at 28 in the mass spectra of $(MX)_nM^+$ alkali halide clusters, it appears that the calculations are slightly more accurate for those clusters, and that the five-atom terrace (27) and vacancy (29) structures become preferred structures for $(MgO)_nMg^{2+}$ clusters at smaller sizes than they do for the alkali halides. There is also a discrepancy between the maxima observed at 10 in the calculations and at 11 in the mass spectra, but other than that there is generally good agreement between our calculations and mass spectra. The results lend further support to our assignments of cluster structures, and also indicate that in spite of quantitative inaccuracies, this simple model provides a useful tool for studying the structural properties of these clusters.

The results of these calculations are more quantitatively accurate for the alkali halides, and suggest that in addition to being responsible for the stable cuboid and terrace structures observed in the mass spectra of laser-vaporized alkali halides, the monomer fragmentation channel may also contribute to the presence of stable vacancy clusters. It is thought that $(MX)_nM^+$ clusters with vacancy structures are produced from cuboid $(MX)_{n+1}$ clusters that once ionized, lose a neutralized halide atom, but then undergo no further fragmentation.[9,12] However, our calculated cluster stabilities indicate that vacancy clusters are quite stable with respect to fragmentation by the loss of monomers, and we observe $(MgO)_nMg^{2+}$ clusters with stable vacancy structures which, for reasons discussed earlier, almost certainly are not formed by the loss of a neutralized O atom from cuboid $(MgO)_{n+1}^{2+}$ clusters.

The $(MgO)_nMg_2^{2+}$ cluster distributions that we observe at 308 nm also exhibit local maxima, and in Fig. 1

we show a cluster distribution obtained in high enough abundances to enable the determination of maxima in the range $12 \leq n \leq 24$. The intensities of $(MgO)_nMg_2^{2+}$ clusters are too low to assign magic numbers with confidence for $n > 24$ and, as discussed earlier, the smallest $(MgO)_nMg_2^{+2}$ cluster is evidently $(MgO)_{12}Mg_2^{2+}$. The maxima occur at 12, 14 or 15, 17, 21, and 23, but because $(MgO)_nMg_2^{2+}$ clusters with even values of n have the same mass-to-charge ratio as singly charged $(MgO)_{n/2}Mg^+$ clusters, and therefore appear at the same place in the mass spectrum, we cannot immediately assume that the maxima correspond to exceptionally stable $(MgO)_nMg_2^{2+}$ clusters. The maxima at 17, 21, and 23 are odd numbers, and therefore correspond to true $(MgO)_nMg_2^{2+}$ magic numbers. The intensities at 12 and 14 probably include contributions from $(MgO)_6Mg^+$ and $(MgO)_7Mg^+$ clusters, and so they are questionable in terms of special abundance. We can gain some idea of the contributions from $(MgO)_6Mg^+$ and $(MgO)_7Mg^+$ clusters by using higher laser power to eliminate the $(MgO)_nMg_2^{2+}$ cluster signal, as long as the $(MgO)_nMg^+$ signal that remains is about the same as that at low power. In Fig. 3 we show mass spectra obtained at two different laser powers. When the power is doubled the peaks corresponding to odd numbered $(MgO)_nMg_2^{2+}$ clusters disappear, indicating that the even numbered clusters are also gone, and that only $(MgO)_nMg^+$ clusters remain. In addition, the intensities of $(MgO)_nMg^+$ clusters either increase or stay about the same for $n \leq 5$ [only $(MgO)Mg^+$ increases significantly], in which range there are no contributions from $(MgO)_nMg_2^{2+}$ clusters at either laser power. This indicates that our use of the $(MgO)_nMg^+$ signal at high power to estimate that at low power is reasonable, but may overestimate the contribution of $(MgO)_nMg^+$ clusters to the $(MgO)_nMg_2^{2+}$ peaks. Since the intensity of $(MgO)_7Mg^+$ is significant, compared to the small difference in the intensities of $(MgO)_{14}Mg_2^{2+}$ and $(MgO)_{15}Mg_2^{2+}$ clusters, its contribution to the $(MgO)_{14}Mg_2^{2+}$ signal is probably enough to shift the maximum from 15 to 14. Furthermore, the $(MgO)_{14}Mg_2^{2+}$ and $(MgO)_{15}Mg_2^{2+}$ peaks in Fig. 1 are almost identical in height [more so than in Fig. 3(a)], indicating that the removal of the slightest $(MgO)_7Mg^+$ contribution would lead to a maximum at 15. On the other hand, the intensity of $(MgO)_6Mg^+$ is small compared to the large difference in the intensities of the $(MgO)_{12}Mg_2^{2+}$ and $(MgO)_{13}Mg_2^{2+}$ clusters, suggesting that 12 is a true magic number. We will therefore propose that the most stable $(MgO)_nMg_2^{2+}$ clusters are those at 12, 15, 17, 21, and 23.

In spite of the uncertainties in our assignments of magic numbers for $(MgO)_nMg_2^{2+}$ clusters, it is worthwhile to consider the cubic structures that might explain their appearance. The structures of $(MgO)_nMg_2^{2+}$ clusters are generally much less stable than those of $(MgO)_nMg^{2+}$ clusters, because the presence of a second excess metal atom requires more O-atom vacancies in the lattice and reduces the number of Mg coordination partners. For example, it is not possible to construct a complete cuboid lattice for a $(MgO)_nMg_2^{2+}$ cluster. The most compact structures that can be obtained in the 12–24 range are $3\times3\times3$ and $5\times3\times3$ cuboids with an interior O-atom vacancy, and they are probably the structures of the clusters responsible for the magic numbers at 12 and 21. The first of these was calculated to have a high stability for $(NaCl)_{12}Na_2^{2+}$ clusters,[3] and the second is a simple extension of this structure. The structures might be even more stable for the $(MgO)_{12}Mg_2^{2+}$ and $(MgO)_{21}Mg_2^{2+}$ clusters than for the doubly charged alkali halides, since $(MgO)_nMg_2^{2+}$ clusters have two excess electrons (from the two extra divalent Mg atoms) that could occupy a vacancy, similar to a solid state F center. The excess electron present in neutral alkali halide clusters that contain one extra metal atom has been shown to provide additional stability to vacancy structures.[10] If the $3\times3\times3-1$ structure is correct for $(MgO)_{12}Mg_2^{2+}$, then the $(MgO)_{15}Mg_2^{2+}$ clusters may have this structure with an added 3×2 terrace. There is no obviously stable structure for $(MgO)_{17}Mg_2^{2+}$ clusters, but a plausible one is a $4\times3\times3-1$ structure in which an O-atom vacancy in the center of a 3×3 face is replaced by a Mg atom, and possibly one or two excess electrons. The most stable structures for $(MgO)_{23}Mg_2^{2+}$ clusters might be a $3\times3\times3$ cube with an added 3×1 railing, or an altered $4\times4\times3-1$ structure similar to that suggested for $(MgO)_{17}Mg_2^{2+}$. Further study of these metal-rich clusters is warranted, and might help to provide an understanding of the structural preferences that develop as metal-metal bonding becomes important.

Mechanism of evaporation

We have not yet studied the fragmentation of MgO clusters in detail, but because they have crystallike structural properties, they probably fragment by a mechanism that is similar to that by which solid materials vaporize. The evaporation of solids has been investigated extensively, and it is commonly thought to occur by a stepwise process in which atoms or molecules move successively from higher to lower binding energy sites, until they eventually desorb.[35,36] This is often referred to as the terrace-ledge-kink (TLK) model. Depending on the experimental conditions (vacuum or equilibrium vaporization, crystal stoichiometry, etc.), one of these steps will be rate limiting, and usually an important aspect of an evaporation study is to try to identify this step. Magnesium oxide has been investigated, and for both equilibrium and vacuum conditions it vaporizes congruently according to the reaction $MgO(s) \rightarrow Mg(g) + \frac{1}{2}O_2(g)$ [plus a small percentage of $MgO(g)$],[37,38] as is typical for II-VI compounds.[39] The details of the process are not well known, but it has been proposed[40] that the movement of atoms or molecules from ledges into an adsorbed layer is quite rapid, and that the evaporation rate is limited by the surface diffusion of adsorbed O atoms. Once two O atoms find each other, they readily combine and desorb along with two Mg atoms. It is known that O_2 adsorbs very weakly to high purity MgO.[41] The evaporation of other II-VI compounds has been studied, and ledge dissociation,[42] electron transfer,[35,43] and desorption[44] all have been proposed as rate-limiting steps.

The predominance of $(MgO)_nMg^{2+}$ clusters in our mass spectra shows that these clusters evaporate by losing Mg and O in equal amounts to form smaller clusters within the same series. This is similar to the congruent vaporization of solid MgO, and is the primary (possibly the only) pathway over most of the cluster distribution. For small clusters other fragmentation channels may be accessible, leading to the $(MgO)_n{}^+$ and $(MgO)_nMg^+$ clusters that appear in the mass spectra [the $(MgO)_nMg_2{}^{2+}$ clusters come from more metal-rich species]. The primary channel for the formation of $(MgO)_n{}^+$ clusters is probably the loss of Mg^+, since small $(MgO)_nMg^+$ clusters ($n \leq 6$) subjected to collision-induced fragmentation lose mostly Mg^+ or Mg, and some MgO.[45] The presence of an extra charge should lead to an even greater loss of Mg^+ from small $(MgO)_nMg^{2+}$ clusters. It is possible that $(MgO)_nMg^{2+}$ clusters also lose $(MgO)Mg^+$ to form $(MgO)_n{}^+$ clusters, since the abundance of $(MgO)Mg^+$ increases significantly at higher laser power (Fig. 3), whereas the intensities of the other $(MgO)_nMg^+$ cluster peaks change very little. The $(MgO)Mg^+$ peak is also very large at 248 nm, and is second in intensity only to Mg^+ (not shown), which is saturated (i.e., intensity > 256 mV) in all of the mass spectra presented here. The $(MgO)_nMg^+$ clusters might be generated by the loss of $Mg^+ + Mg + O_2$, or MgO^+ from $(MgO)_nMg^{2+}$ clusters, or by the loss of Mg^+ or $(MgO)Mg^+$ from small $(MgO)_nMg_2{}^{2+}$ clusters.

If the singly charged clusters observed under low flow conditions are formed primarily by the fragmentation of doubly charged clusters, rather than by the single ionization of neutral clusters, then the largest $(MgO)_n{}^+$ and $(MgO)_nMg^+$ clusters observed in our mass spectra indicate that these channels begin to open up once n decreases to about 20. If clusters formed by single ionization are in important contribution to the signal, then the actual onset due to fragmentation may occur at somewhat smaller sizes. Because the intensities of $(MgO)_nMg^{2+}$ clusters decrease rather sharply when n is less than about 8–12, and the singly charged cluster signal usually increases substantially in the same region (modulated by the usual magic number patterns for these clusters), the channels leading to $(MgO)_n{}^+$ and $(MgO)_nMg^+$ clusters appear to be most easily accessible for about $n \leq 12$. By the time n reaches 4, $(MgO)_nMg^{2+}$ clusters fragment solely to singly charged clusters, since no smaller $(MgO)_nMg^{2+}$ clusters are observed. This is evidently the approximate cluster size at which the height of the fission barrier, which must be overcome to form singly charged fragments, becomes equal to the energy required to evaporate neutrals.[20] In the more weakly bound $(MgO)_nMg_2{}^{2+}$ clusters this equality occurs at about 12.

If, like the solid, Mg atoms and O_2 molecules are the primary species desorbed from $(MgO)_nMg^{2+}$ clusters (rather than MgO molecules), then one possible TLK mechanism for the evaporation of the clusters is

$$(MgO)_{\text{corner}} \rightarrow (MgO)_{\text{ads}} \quad \text{(cuboid)}$$

$$(MgO)_{\text{corner kink}} \rightarrow (MgO)_{\text{ads}} \quad \text{(O-atom vacancy)}$$

$$(MgO)_{\text{terrace corner}} \rightarrow (MgO)_{\text{ledge}} \rightarrow (MgO)_{\text{ads}} \quad \text{(complete terrace)}$$

$$(MgO)_{\text{terrace kink}} \rightarrow (MgO)_{\text{ledge}} \rightarrow (Mg)_{\text{ads}} \quad \text{(intermediate)}$$

$$(MgO)_{\text{ads}} \rightarrow (Mg+O)_{\text{ads}} \rightarrow (Mg+\tfrac{1}{2}O_2)_{\text{ads}} \rightarrow (Mg+\tfrac{1}{2}O_2)_{\text{vapor}}$$

where the subscripts refer to the sites occupied by the atoms or molecules (Fig. 5). The first four lines correspond to the steps involved in the movement of a MgO molecule into the adsorbed layer of the cuboid, O-atom vacancy, complete terrace, and intermediate (i.e., a structure other than one of the three exceptionally stable types) clusters, and the last line is the series of steps proposed to occur in the adsorbed layer of all the clusters prior to desorption. The major difference in the evaporation mechanism proposed for each cluster is the first step, for which the initial and final sites occupied by a MgO molecule are designated by the first arrrow. By using the results of our ionic-model calculations and assuming that the energy required to move a MgO molecule from one site to another is equal to the difference in the potential energy of the cluster before and after the move, we estimate that the average energy required for the first step is 2.35, 1.59, 0.85, and 0.23 eV, for the four cluster types, respectively. These numbers can only be used qualitatively, but they do predict the same order of stability as observed in the mass spectra, suggesting that such a mechanism is plausible.

There are certainly other possible evaporation mechanisms, but choosing from among them would require additional experimental data and more accurate calculations than we can make with this simple ionic model. For example, it may be that in the mechanism shown above, the Mg and O atoms detach separately from corners, kinks, and ledges, rather than as MgO mole-

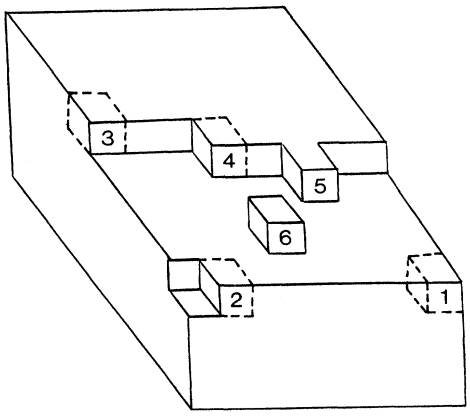

FIG. 5. Simple model of the surface of a MgO cluster that has the fcc structure of crystalline MgO. The labeled sites are (1) corner, (2) corner kink, (3) terrace corner, (4) terrace kink, (5) ledge, and (6) adsorbed layer.

cules. Furthermore, because the Mg and O atoms in a cluster are charged, whereas those in the proposed desorption products are neutral, charge transfer might play an important role. At some point during evaporation, the Mg^{z+} and O^{z-} ions must gain and lose electrons, respectively, if they are to desorb as Mg atoms and O_2 molecules. Charge transfer may not be so important if MgO molecules desorb, because then the charges on the ions must only shift from the cluster values to the molecule values of about ± 0.74 (calculated from the dipole moment and bond length of the molecule), rather than become neutralized. Alkali halide crystals vaporize this way, such that monomers and dimers are lost through a TLK mechanism in which the rate-limiting step is thought to be the movement of monomers and dimers from kinks and ledges into the adsorbed layer.[46] Alkali halide $(MX)_n M^+$ clusters probably evaporate by a similar TLK mechanism, since they also evaporate primarily monomers and dimers. The most likely $(MgO)_n Mg^{2+}$ clusters to desorb MgO molecules are those for which the product cluster would be extremely stable, such as the $(MgO)_{37}Mg^{2+}$ cuboid cluster that could be formed by the loss of a MgO molecule from $(MgO)_{38}Mg^{2+}$. The abundance minima that appear for clusters with one MgO molecule more than the cuboid clusters are evidence for this pathway. We cannot identify the species that desorb from $(MgO)_n Mg^{2+}$ clusters by using the results presented here, but we have recently added a reflection and a quadrupole mass spectrometer equipped with an electron impact ionizer (to detect O_2) that should make this possible.

Regardless of the details of the TLK mechanism of evaporation of $(MgO)_n Mg^{2+}$ [and also $(MgO)_n Mg^+$ and $(MgO)_n{}^+$] clusters, and without the need for calculations, our mass spectra provide us with important information about the factors that control evaporation. Because the magic numbers in the mass spectra are due to differences in cluster evaporation rates that result from differences in cluster stabilities, and because they depend on the structural properties of the clusters, the movement of atoms or molecules from corners, kinks, and ledges must play some role in determining the rate of evaporation. If these steps were not important, and the rate depended entirely on some later step, such as diffusion or desorption, then there would be no reason for the magic numbers (if they even appeared in this case) to depend on cluster structure. Any differences in evaporation rates due to structural properties would be unobservable, since the time required for the initial steps would be a negligible contribution to the total time of an evaporation event. These initial steps are therefore either rate limiting, or they exert partial control over the evaporation rate by affecting the concentration of atoms or molecules in the adsorbed layer.

CONCLUSIONS

In these experiments, doubly charged $(MgO)_n Mg^{2+}$ clusters are formed from more metal-rich clusters which are first doubly ionized and then desorb excess Mg atoms until they attain a nearly stoichiometric composition. The $(MgO)_n Mg^{2+}$ clusters then evaporate Mg and O in equal amounts, probably as $2Mg + O_2$ and MgO, similar to the congruent vaporization of solid MgO. Fragmentation channels leading to singly charged clusters apparently become accessible as n decreases to about 20, and eventually lead to the complete absence of $(MgO)_n Mg^{2+}$ clusters for $n < 4$. As a result of fragmentation, magic numbers appear in the mass spectra corresponding to clusters with exceptionally stable structures. The observed pattern of magic numbers shows that $(MgO)_n Mg^{2+}$ clusters have cubic structures resembling pieces of the MgO fcc crystal lattice, with the most stable structures being cuboids, and cuboids with an O-atom vacancy or a complete terrace. Similar structures can be used to explain the abundances of $(MgO)_n Mg_2{}^{2+}$ clusters, but in this case the O-atom vacancies may be occupied by one or two excess electrons. The evaporation of MgO clusters probably occurs by a stepwise TLK mechanism in which atoms or molecules move successively from higher to lower binding energy sites, until they eventually desorb. The presence of magic numbers in the mass spectra shows that the initial movement of species from corners, kinks, and ledges must either be rate limiting, or exert partial control over the evaporation rate by affecting the concentration of atoms or molecules in the adsorbed layer. The conclusions drawn here are consistent not only with the experimental data presented, but also with the results of our ionic-model calculations, showing again the utility of such calculations for obtaining qualitative information on MgO clusters.

ACKNOWLEDGMENTS

We gratefully acknowledge the E. I. DuPont de Nemours and Company for an unrestricted grant through the Department of Chemistry, and one of us (P.J.Z.) thanks them for their financial support through the Pennsylvania State University Particle Science and Technology Center. The authors also thank Dr. R. W. Farley and Dr. R. G. Keesee for helpful discussions during the course of this work.

[1]T. D. Märk and A. W. Castleman, Jr., *Advances in Atomic Molecular Phyiscs* (Academic, New York, 1985), Vol. 20, p. 65.

[2]A. W. Castleman, Jr. and R. G. Keesee, Ann. Rev. Phys. Chem. **37**, 25 (1986).

[3]T. P. Martin, Phys. Rep. **95**, 167 (1983).

[4]K. Sattler, J. Muhlbach, O. Echt, P. Pfau, and E. Recknagel, Phys. Rev. Lett. **47**, 160 (1981).

[5]T. M. Barlak, J. E. Campana, J. R. Wyatt, and R. J. Volton, J. Phys. Chem. **87**, 3441 (1983).

[6]W. Ens, R. Beavis, and K. G. Standing, Phys. Rev. Lett. **50**, 27 (1983).

(1983).
[7]R. Pflaum, P. Pfau, K. Sattler, and E. Recknagel, Surf. Sci. **156**, 165 (1985).
[8]R. Pflaum, K. Sattler, and E. Recknagel, in *Physics and Chemistry of Small Clusters,* edited by P. Jena, B. K. Rao, and S. N. Khanna (Plenum, New York, 1987), p. 103.
[9]C. W. S. Conover, Y. A. Yang, and L. A. Bloomfield, Phys. Rev. B **38**, 3517 (1988).
[10]E. C. Honea, M. L. Homer, P. Labastie, and R. L. Whetten, Phys. Rev. Lett. **63**, 394 (1989).
[11]H. J. Hwang, D. K. Sensharma, and M. A. El-Sayed, J. Phys. Chem. **93**, 5012 (1989).
[12]Y. J. Twu, C. W. S. Conover, Y. A. Yang, and L. A. Bloomfield, Phys. Rev. B **42**, 5306 (1990).
[13]D. O. Welch, O. W. Lazareth, G. J. Dienes, and R. D. Hatcher, J. Chem. Phys. **68**, 2159 (1978).
[14]J. Diefenbach and T. P. Martin, Surf. Sci. **156**, 234 (1985).
[15]P. J. Ziemann and A. W. Castelman, Jr., J. Chem. Phys. **94**, 718 (1991).
[16]*Chemical and Mechanical Behavior of Inorganic Materials,* edited by A. W. Searcy, D. V. Ragone, and U. Colombo (Wiley, New York, 1970).
[17]K. Aika and J. H. Lunsford, J. Phys. Chem. **81**, 1393 (1977).
[18]B. Henderson and J. E. Wertz, *Defects in Alkaline Earth Oxides* (Wiley, New York, 1977).
[19]O. Echt, in *Physics and Chemistry of Small Clusters,* edited by P. Jena, B. K. Rao, and S. N. Khanna (Plenum, New York, 1987), p. 623.
[20]W. A. Saunders, Phys. Rev. Lett. **64**, 3046 (1990).
[21]C. Bréchignac, Ph. Cahuzac, F. Carlier, and M. de Frutos, Phys. Rev. Lett. **64**, 2893 (1990).
[22]R. W. Farley, P. J. Ziemann, and A. W. Castleman, Jr., Z. Phys. D **14**, 353 (1989).
[23]M. Matsui, J. Chem. Phys. **91**, 489 (1989).
[24]M. F. C. Ladd and W. H. Lee, Acta Crystallogr. **13**, 959 (1960).
[25]S. Sasaki, K. Fujino, Y. Takéuchi, Proc. Jpn. Acad. **55**, 43 (1979).
[26]M. Causá, R. Dovesi, C. Pisani, and C. Roetti, Acta Crystallogr. Sec. B **42**, 247 (1986).
[27]*CRC Handbook of Chemistry and Physics,* 63rd ed., edited by R. C. Weast and M. J. Astle (Chemical Rubber Company, Boca Raton, FL, 1982-1983).
[28]R. S. Berry, S. A. Rice, and J. Ross, *Physical Chemistry* (Wiley, New York, 1980), pp. 569–571.
[29]G. H. Reiling and E. B. Hensley, Phys. Rev. **112**, 1106 (1958).
[30]G. C. Nieman, E. K. Parks, S. C. Richtsmeier, K. Liu, L. G. Pobo, and S. J. Riley, High Temp. Sci. **22**, 115 (1986).
[31]I. Katakuse, T. Ichihara, H. Ito, and M. Hirai, Rapid Commun. Mass Spectrom. **1**, 16 (1990).
[32]L. Operti, E. C. Tews, T. J. MacMahon, and B. S. Freiser, J. Am. Chem. Soc. **111**, 9152 (1989).
[33]T. P. Martin and T. Bergmann, J. Chem. Phys. **90**, 6664 (1989).
[34]P. J. Ziemann and A. W. Castleman, Jr. (unpublished).
[35]G. A. Somorjai and J. E. Lester, Progr. Solid State Chem. **4**, 1 (1967).
[36]O. Knacke and I. N. Stranski, Progr. Metal Phys. **6**, 181 (1956).
[37]A. W. Searcy, in *Chemical and Mechanical Behavior of Inorganic Materials,* edited by A. W. Searcy, D. V. Ragone, and U. Colombo (Wiley, New York, 1970), p. 57.
[38]R. L. Altman and A. W. Searcy, Abstracts of Scientific Papers at the XVIII International Congress of Pure and Applied Chemistry (University of Toronto Press, Toronto, 1961), p. 100.
[39]M. S. Chandrasekharaiah, in *The Characterization of High Temperature Vapors,* edited by J. L. Margrave (Wiley, New York, 1967), Appendix B, p. 495.
[40]M. Peleg and C. B. Alcock, High Temp. Sci. **6**, 52 (1974).
[41]R. L. Nelson, A. J. Tench, and B. J. Harmsworth, J. Trans. Faraday Soc. **63**, 1427 (1967).
[42]Z. A. Munir, L. S. Seacrist, and J. P. Hirth, Surf. Sci. **28**, 357 (1971).
[43]G. A. Somorjai and J. E. Lester, J. Chem. Phys. **43**, 1450 (1965).
[44]R. J. Galluzzo and A. W. Searcy, High Temp. Sci. **3**, 491 (1971).
[45]W. A. Saunders, Phys. Rev. B **37**, 6583 (1988).
[46]J. E. Lester and G. A. Somorjai, J. Chem. Phys. **49**, 2940 (1965).